Effect of Gd Substitution on Structural and Magnetic Properties of Mn-Ni-Zn Ferrites

Md. Nazrul Islam[a,b]

Abstract— Structural and magnetic properties of $Mn_{0.5}Ni_{0.1}Zn_{0.4}Fe_{2-x}Gd_xO_4$ (where x = 0.0, 0.015, 0.03, 0.06, and 0.1) sintered at 1250ºC for 3 hours are investigated thoroughly.The samples are prepared by standard solid state reaction technique.X-ray diffraction(XRD) patterns confirm the formation of single phase spinel structure. SEM micrographs show that the average grain size decreases with increasing Gd content. The initial permeability shows similar trend as average grain size with the variation of Gd content. The magnetic loss is found to decrease with increasing frequency up to 1 MHz and beyond this frequency, magnetic loss increases with the frequency. It is also observed that the value of magnetic loss for the Gd substituted compositions is comparably less than the parent composition at frequency greater than 1 MHz. The saturation magnetization (M_S) value increases initially for x = 0.015. Beyond this value of x, M_S is decreased with increase in Gd content.

Keywords— Grain size, Loss tangent, Lattice parameter, Microstructure, Relative quality factor, Spinel ferrites, Yafet-Kittle angle.

1 Introduction

During the last few decades, spinel ferrites are widely used in many electronic devices. These are preferred because of their high permeability in the radio-frequency (RF) region, high electrical resistivity, mechanical hardness, chemical stability, and reasonable cost [1–4]. Ferrites are also useful to prevent and eliminate RF interference to audio systems. According to their structure, they have tetrahedral A-site and octahedral B-sites in AB_2O_4 crystal structure. These materials show various magnetic properties depending on the cation distribution of the chemical compositions. Various cations can be placed in A-site and B-sites to tune their magnetic properties [2–11]. From the application point of view, both Mn–Zn and Ni–Zn ferrites have a great importance, where they are used in many ferrite devices such as magnetic heads, converters, electromagnetic wave absorbers, and inductor cores. Though Mn–Zn ferrites have distinctive magnetic properties as high magnetization and initial permeability, they have comparatively high power losses and low electrical resistivity at high frequencies. In contrast, Ni–Zn ferrites are characterized by their low dielectric loss, high resistivity and high Curie temperature, but they have comparatively low initial permeability at high frequencies. Combinations between these two ferrites were carried out by many researchers trying to obtain favorable magnetic properties with low losses especially at high frequencies [12–17].

In a previous study, the magnetic and electrical properties of such a combination were investigated [18, 19]. The sample with the chemical formula $Mn_{0.5}Ni_{0.1}Zn_{0.4}Fe_2O_4$ was found to possess the optimum properties for promising applications. In addition, it was noticed clearly that the properties of Mn–Ni–Zn ferrites are predominantly governed by the type of substituted ions [13, 14, 19]. Accordingly, the present research directed to investigate the effect of Gd^{3+} substitution on structural and magnetic properties of $Mn_{0.5}Ni_{0.1}Zn_{0.4}Fe_{2-x}Gd_xO_4$ prepared by solid state reaction technique.

- [a] *Department of Physics, Bangladesh University of Engineering and Technology (BUET), Dhaka 1000, Bangladesh.*
- [b] *Faculty of Science & Humanities, Bangladesh Army International University of Science & Technology (BAIUST), Comilla Cantonment, Comilla, Bangladesh. PH: +8801716474658, +8801813676151. E-mail: mnazrul_cu@yahoo.com, nazrul_physics@baiust.edu.bd*

2 Experimental

2.1 Sample Preparation

The Gd substituted various $Mn_{0.5}Ni_{0.1}Zn_{0.4}Fe_{2-x}Gd_xO_4$ with x = 0.0, 0.015, 0.03, 0.06 and 0.1 were prepared by the standard solid state reaction technique. Commercially available powders of $MnCO_3$ (99.9%), NiO (99.9%), ZnO (99.9%), Gd_2O_3 (99.95%) and Fe_2O_3 (99.9%) were used as raw materials. Stoichiometric amounts of required powders were weighed and mixed thoroughly in acetone media using an agate mortar for 4 h. Then the well mixed powders were calcined at 900ºC in a closed alumina crucible for 5 h. The calcined powders were grinded thoroughly again for 3 h to obtain a homogeneous mixture. Later the powders were mixed with 10% polyvinyl alcohol (PVA) as a binder for granulation. Then the powders were pressed uniaxially at a pressure of about 45 MPa into pellet shaped (about 13 mm diameter, 1.5-2.0 mm thickness) and toroid shaped (about 13 mm outer diameter, 6-7 mm inner diameter, and 2.0-2.5 mm thickness) samples. Finally the samples were sintered at 1250ºC in air for 3 h. During sintering process, the temperature ramp was 10ºC/min for heating and 5ºC/min for cooling.

2.2 Characterizations

The crystal structure of the prepared samples were studied using an X-ray diffractometer (Philips PANalytical

X'PERT-PRO) with CuKα radiation (λ = 1.541 Å) at room temperature. XRD patterns of all samples were collected over a range of 2θ from 20° to 60° using a step size 0.04°. The bulk density (ρ_B) for each sample was calculated using the relation, $\rho_B = m/(\pi r^2 t)$, where m is the mass, r is the radius and t is the thickness of the pellet. The theoretical density (ρ_{th}) was calculated using the relation, $\rho_{th} = 8M/(N_A a_0^3)$, where M is the molecular weight of the composition, N_A is the Avogadro's number, and a_0 is the lattice constant. The porosity (P) was calculated using the formula, $P = [100(\rho_{th} - \rho_B)/\rho_{th}]\%$. Microstructure and surface morphology of the sintered samples were performed by Field Emission Scanning Electron Microscope (FESEM, Model no.: JEOL JSM-7600F). Average grain sizes (grain diameter) of the samples were determined from FESEM images by linear intercept technique [20]. The real part (μ_i') and imaginary part (μ_i'') of the complex initial permeability were measured as a function of frequency within the range of 100 Hz to 120 MHz using a WAYNE KERR 6500B Impedance Analyzer. The values of μ_i' and μ_i'' were calculated using the relations: $\mu_i' = L_S/L_0$ and $\mu_i'' = \mu_i' \tan\delta_M$, where L_S is the self inductance of the sample core and L_0 is the inductance of the winding coil without the sample core and $\tan\delta_M$ is the magnetic loss. L_0 is derived geometrically using the relation, $L_0 = \mu_0 N^2 S/\pi\bar{d}$, where μ_0 is the permeability in vacuum, N is the number of turns of the coil (N = 5), S is the cross-sectional area and $\bar{d} = (d_1 + d_2)/2$ is the mean diameter of the toroid-shaped sample, where d_1 and d_2 are the inner and outer diameter of the toroid-shaped sample, respectively [3]. The relative quality factor (RQF) was calculated from the relation, $RQF = \mu_i'/\tan\delta_M$. The magnetic hysteresis loops (M-H curves) were measured using a vibrating sample magnetometer (VSM, Model no.: Micro Sense, EV9) at room temperature.

3 Results and Discussion

3.1 XRD analysis, Density and Porosity

One of the most fundamental studies used to characterize the structure of materials is X-ray diffraction (XRD). The X-ray diffraction has been performed to verify the phase formation of various $Mn_{0.5}Ni_{0.1}Zn_{0.4}Fe_{2-x}Gd_xO_4$ sintered at 1250°C. Fig. 1 shows the XRD patterns of $Mn_{0.5}Ni_{0.1}Zn_{0.4}Fe_{2-x}Gd_xO_4$ with x = 0.0, 0.015, 0.03, 0.06 and 0.1 for the angle of 2θ from 20° to 60°. The peaks observed in the XRD patterns are indexed with their Miller indices for (220), (311), (222), (400), (422), and (511) planes. Positions of the peaks comply with the reported value [21, 22]. The XRD patterns for these compositions confirm the formation of spinel structure.

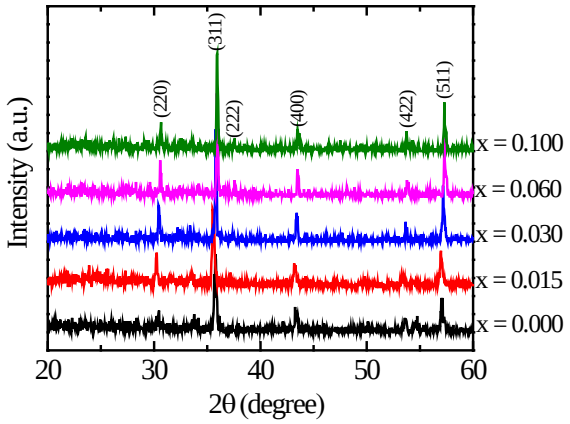

Fig. 1. The X-ray diffraction patterns for various $Mn_{0.5}Ni_{0.1}Zn_{0.4}Fe_{2-x}Gd_xO_4$.

The values of lattice parameter (a) obtained from each crystal plane are plotted against Nelson-Riley function, $F(\theta) = \frac{1}{2}[(\cos2\theta/\sin\theta) + (\cos2\theta/\theta)]$; where θ is the Bragg's angle, and a straight line is obtained. The exact lattice parameter (a_o) for each compositions is determined from the extrapolation of these lines with F(θ) = 0. The calculated a_o for various $Mn_{0.5}Ni_{0.1}Zn_{0.4}Fe_{2-x}Gd_xO_4$ are plotted as a function of Gd content, as shown in Fig. 2. It is found that the exact lattice parameter decreases with the Gd content up to x = 0.03 then it increases with the increase of Gd content. Similar trend has been found for Nd substituted Mn-Ni-Zn ferrites [14]. For $x \le 0.03$, the decrease in the exact lattice parameter could be attributed to that some rare earth ions reside at the grain boundaries. Therefore, they hinder the grain growth and may exert a pressure on the grains and lead the exact lattice parameter to decrease. On the other side, for $x > 0.03$, some of the Gd^{3+} (radius = 0.97 Å) that substitute Fe^{3+} (radius = 0.64 Å) in the unit cell may cause the increase in the exact lattice parameter which in turn compensates the decrease due to the grain boundaries pressure.

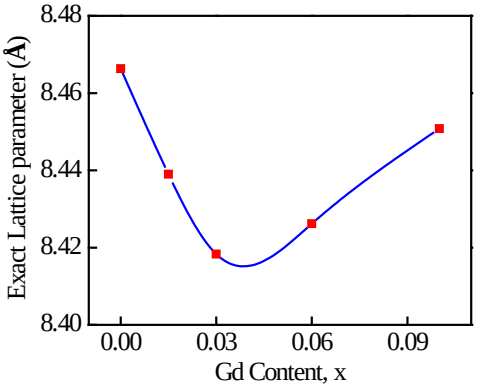

Fig. 2. The variation of exact lattice parameter with Gd content for various $Mn_{0.5}Ni_{0.1}Zn_{0.4}Fe_{2-x}Gd_xO_4$.

Fig. 3 shows the variation of bulk density and porosity

with Gd content for various $Mn_{0.5}Ni_{0.1}Zn_{0.4}Fe_{2-x}Gd_xO_4$. It is observed that as Gd content increases in $Mn_{0.5}Ni_{0.1}Zn_{0.4}Fe_{2-x}Gd_xO_4$, bulk density decreases. It is possible to explain this phenomenon in terms of the porosity and SEM analysis. Porosity (P) of all compositions increases with increasing Gd concentration, as shown in Fig. 3. From the SEM analysis, it is also observed that the number of pores and hence pore volume increase with the increase of Gd content which will be discussed in next section.

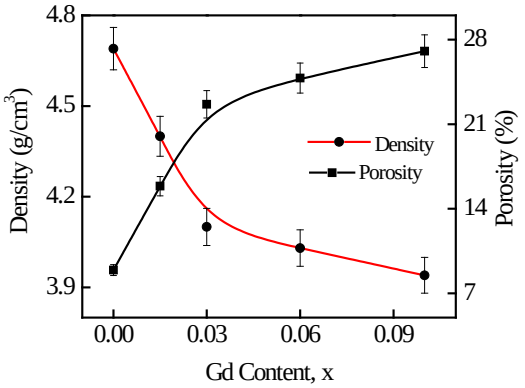

Fig. 3. The variation of density and porosity with Gd contents for various $Mn_{0.5}Ni_{0.1}Zn_{0.4}Fe_{2-x}Gd_xO_4$.

3.2 Microstructure (Surface Morphology)

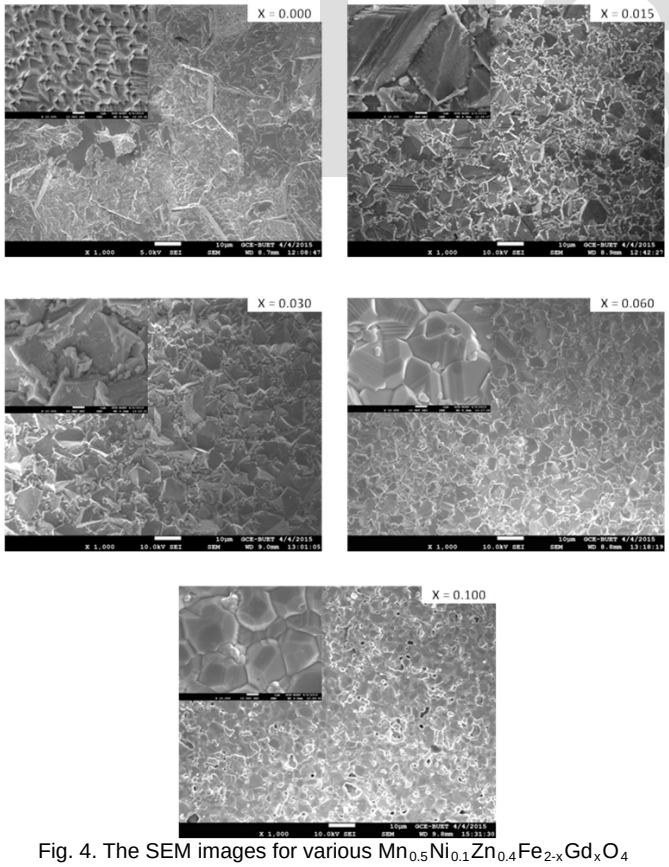

Fig. 4. The SEM images for various $Mn_{0.5}Ni_{0.1}Zn_{0.4}Fe_{2-x}Gd_xO_4$ (each inset shows 10 times enlarged image of the same composition).

The microstructural study has been performed in order to have an insight of the grain structures. The samples of different compositions are chosen for this purpose. The sample is investigated using FESEM. Average grain sizes (grain diameter) of the samples are determined from SEM micrographs by linear intercept technique. To do this, several random horizontal and vertical lines are drawn on the micrographs. Then, the number of intersected grains is counted and the length of the line traversed along the grains is measured. Finally the average grain size is calculated by the formula simply total length of the lines and total number of grains ratio. The SEM images of various $Mn_{0.5}Ni_{0.1}Zn_{0.4}Fe_{2-x}Gd_xO_4$ sintered at 1250°C are shown in Fig. 4. In each image, there is an inset image and each inset has been showed 10 times enlarged image of the same sample. It is clear from the SEM images that average grain size goes on decreasing with the Gd content. The average grain size decreases due to the interaction of grain boundary and pores. From the section 3.1, it is observed that the porosity increases with increasing Gd content. So, grain growth is impeded due to the presence of many pores [23].

3.3 Complex Initial Permeability

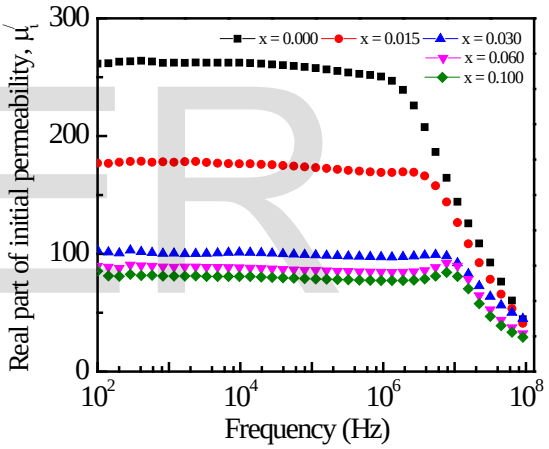

Fig. 5. Variation of μ' as a function of frequency for various $Mn_{0.5}Ni_{0.1}Zn_{0.4}Fe_{2-x}Gd_xO_4$.

The magnetic spectra (initial permeability versus frequency) reflect the properties of inductors [24]. The complex initial permeability is given by $\mu^* = \mu' - i\mu''$. The μ' describes the stored energy expressing the component of magnetic induction B in phase with the alternating magnetic field H. The μ'' describes the dissipation of energy expressing the component of B at 90° out of phase with the alternating magnetic field H. The initial permeability of polycrystalline ferrite materials depends strongly on the domain structure. The magnetic domain structure can be modified either by annealing the sample at suitable temperatures, or by applying an external magnetic field. Fig. 5 shows the frequency dependent real part of initial permeability spectra for various $Mn_{0.5}Ni_{0.1}Zn_{0.4}Fe_{2-x}Gd_xO_4$ sintered at 1250°C. The initial permeability has been measured for all the compositions in the frequency range of 100Hz to 120MHz. The real part of initial

permeability spectra show that μ_i' remains fairly constant up to a certain frequency range, while at higher frequency it drops rapidly to a very small value. The μ_i' is found to decrease with increasing Gd content as shown in Fig. 5. It is due to decrease in density and average grain size with Gd content. From previous section, it is observed that average grain size decreases with the increase of Gd content. It is generally believed that smaller the grain size, lower the saturation magnetization and the initial permeability. In the present investigation, the saturation magnetization is also found to decrease with increasing Gd content which will be discussed in the section 3.5. Since μ_i' is a function of magnetization therefore, μ_i' decreases with the increase of Gd content. Thus, variation of the μ_i' has been found to correlate with its density, average grain size and DC magnetization property.

3.4 Magnetic Loss and Relative Quality Factor

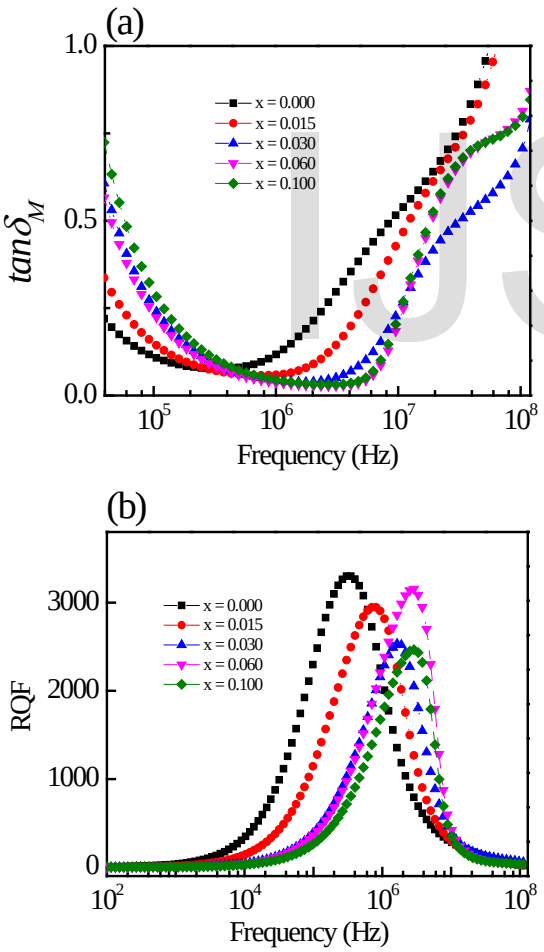

Fig. 6. The variation of (a) magnetic loss ($\tan\delta_M$) and (b) relative quality factor (RQF) with frequency for various $Mn_{0.5}Ni_{0.1}Zn_{0.4}Fe_{2-x}Gd_xO_4$.

The variation of magnetic loss ($tan\delta_M = \mu_i''/\mu_i'$) with frequency for all samples has been studied. Fig. 6(a) shows the variation of $\tan\delta_M$ with frequency for various $Mn_{0.5}Ni_{0.1}Zn_{0.4}Fe_{2-x}Gd_xO_4$ sintered at 1250°C. It is seen from the figure that the $\tan\delta_M$ decreases with increasing frequency up to 1 MHz and beyond this frequency, $\tan\delta_M$ increases with the frequency. It is also observed that the value of $\tan\delta_M$ for the Gd substituted samples is comparably less than the un-substituted samples at frequency greater than 1 MHz. At lower frequencies, a decrease in magnetic loss is observed. The lag of domain wall motion with respect to the applied magnetic field is responsible for magnetic loss and this is accredited to lattice imperfections [25]. At higher frequencies, an increase in loss factor is observed. A resonance loss peak is seen in this increase of magnetic loss. At the resonance, maximum energy transfer occurs from the applied field to the lattice which results the rapid increases in loss factor. As it is observed that phase lag between domain rotation and applied field is greater than that between applied field and domain wall displacement, the magnetic losses due to domain rotation overrides those due to domain wall displacement [26].

The RQF were calculated by the ratio real part of initial permeability and magnetic loss tangent measured on the coil wound toroidal samples. The variation of the RQF with frequency showed almost similar trend for all the samples. Fig. 6(b) shows the variation of RQF with frequency for various $Mn_{0.5}Ni_{0.1}Zn_{0.4}Fe_{2-x}Gd_xO_4$ sintered at 1250°C. By increasing Gd content, the RQF decreases and the peak associated with the RQF shifting to higher frequencies. This phenomenon is associated with the Snoek's law [27]. According to Snock's law, a decrease in initial permeability leads to a increase in the resonance frequency and vice versa.

3.5 DC magnetization

The magnetization as a function of applied magnetic field for various $Mn_{0.5}Ni_{0.1}Zn_{0.4}Fe_{2-x}Gd_xO_4$ at room temperature is shown in Fig. 7. The magnetization of all samples increases sharply with increasing applied magnetic field up to 0.1 T (in $\mu_0 H$). Beyond this applied field, the magnetization increases slowly and then saturation occurs. Therefore, it confirms that all samples show the behavior of soft ferrites at room temperature. The saturation magnetization (M_S) for all the samples determined by the extrapolation of the magnetization curve to $\mu_0 H = 0$. Fig. 8 shows the variation of saturation magnetization as a function of Gd-content. It is seen that the value of M_S slightly increases for x = 0.015 and then it decreases with increasing Gd-content.

The observed variation in M_S can be explained on the basis of cation distribution and exchange interaction between A and B sites. According to the site occupancy preference [28] it is well known that Ni^{2+} and Gd^{3+} prefer octahedral (B) site occupation whereas Zn^{2+} prefer tetrahedral (A) site. 80% of Mn^{2+} occupy the A site while 20% occupy the B-site. Fe^{3+} can exist at both sides though they have preference for the octahedral site. Therefore, the cation distribution of various $Mn_{0.5}Ni_{0.1}Zn_{0.4}Fe_{2-x}Gd_xO_4$ assumed as

$$(Zn_{0.4}^{2+}Mn_{0.4}^{2+}Fe_{0.2}^{3+})[Ni_{0.1}^{2+}Mn_{0.1}^{2+}Gd_x^{3+}Fe_{1.8-x}^{3+}]$$

where the brackets ( ) and [ ] denote A- and B-sites, respectively.

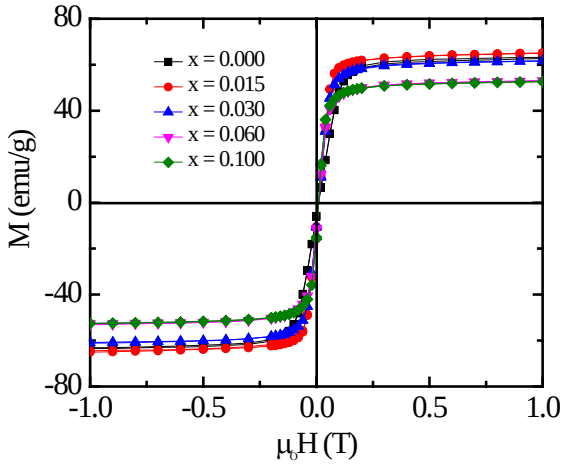

Fig. 7. The variation of magnetization with applied magnetic field for various $Mn_{0.5}Ni_{0.1}Zn_{0.4}Fe_{2-x}Gd_xO_4$.

In ferrites, the magnetic moment arises mainly from the parallel uncompensated electron spin of individual ion. The intensity of magnetization can thus be explained by considering the metal ion distribution and antiparallel spin alignment of the two sublattice sites as given by Neel's model [29]. According to Neel's model, three types of interactions A-A, A-B and B-B are present; with the inter sub lattice A-B super exchange interaction is the strongest one of them and the saturation magnetization is given by the vector sum of the magnetic moments of the individual A and B sublattices i.e. $M_S = M_B - M_A$. Since Zn^{2+} are non-magnetic, the contribution to the magnetization will be mainly due to Mn^{2+}, Ni^{2+}, Fe^{3+}, and Gd^{3+} having magnetic moments of 5, 2, 5, and 7 μ_B, respectively results the net magnetic moment which can be written by,

$$M_B - M_A = (9.7 + 2x)\,\mu_B - 3\,\mu_B$$
$$= (6.7 + 2x)\,\mu_B$$

where,

$M_B = 0.1\times 2\mu_B + 0.1\times 5\mu_B + x\times 7\mu_B + (1.8-x)\times 5\mu_B = (9.7 + 2x)\,\mu_B$

and $M_A = 0.4\times 0\mu_B + 0.4\times 5\mu_B + 0.2\times 5\mu_B = 3\,\mu_B$.

Therefore, M_S is expected to increase as Gd content increases. However, the M_S decreases at higher Gd content, x > 0.015. As Gd content increases, A-B interaction weakens and the canting of the spins gives rise to Yafet-Kittle angle (α_{Y-K}) which is compared to the strength of A-B and B-B exchange interaction [30-32]. Fig. 8 shows α_{Y-K} and M_S as a function of Gd content. The α_{Y-K} is calculated at room temperature by using formula [30, 33]: $n_B = M_B(x)\cos\alpha_{Y-K} - M_A(x)$. The number of Bohr magneton (n_B) has been calculated using the relation, $n_B = (M_w M_S)/(N_A \mu_B)$ [33], where M_S is the saturation magnetization, M_w is the molecular weight, N_A is the Avogadro's number and μ_B is the Bohr magneton. It is seen that the α_{Y-K} increases for samples with Gd content, x > 0.015. Thus, one can conclude that the increase in α_{Y-K} is attributed to the increased favour of triangular spin arrangement on B-sites [31]. This leads to reduce the A-B exchange interaction and subsequent decreases in M_S.

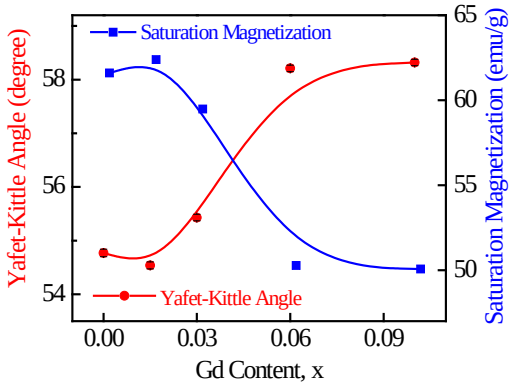

Fig. 8. The variation of saturation magnetization (M_S) and Yafet-Kittle angle (α_{Y-K}) as a function of Gd content for various $Mn_{0.5}Ni_{0.1}Zn_{0.4}Fe_{2-x}Gd_xO_4$.

4 Conclusion

Various $Mn_{0.5}Ni_{0.1}Zn_{0.4}Fe_{2-x}Gd_xO_4$ compositions are successfully synthesized by standard solid state reaction technique. The XRD patterns for these compositions confirm the formation of spinel structure. The value of a_o decreases with the Gd content up to x = 0.03 and then a_o goes up. Bulk density of various $Mn_{0.5}Ni_{0.1}Zn_{0.4}Fe_{2-x}Gd_xO_4$ decreases and porosity increases with the increase of Gd content. The average grain size goes on decreasing with the Gd content. The real part of initial permeability is found to decrease with the substitution of Gd content. The magnetic loss decreases with increasing frequency up to 1MHz and beyond this frequency magnetic loss increases with the frequency. It is also observed that the value of magnetic loss for the Gd substituted samples is comparably less than the un-substituted samples at frequency greater than 1 MHz. It is found that with the increase of Gd content, the RQF decreases and the peak associated with this shifted to higher frequencies. The variation of magnetization with applied magnetic field for various $Mn_{0.5}Ni_{0.1}Zn_{0.4}Fe_{2-x}Gd_xO_4$ confirms that all compositions show the behavior of soft ferrites at room temperature. It is seen that the M_S slightly increases for the sample with x = 0.015 and then it decreases with increasing Gd-content.

Acknowledgment

I sincerely acknowledge the CASR Grant no. 256(19), Bangladesh University of Engineering and Technology

(BUET), Bangladesh to provide financial support for this research.

REFERENCES

[1] R. Peelamedu, C. Grimes, D. Agrawal, R. Roy, "Ultralow dielectric constant nickel–zinc ferrites using microwave sintering", J. Mater. Res., vol. 18, p. 2292, 2003.

[2] A. K. M. Akther Hossain, S. T. Mahmud, M. Seki, T. Kawai, H. Tabata, "Structural, electrical transport, and magnetic properties of $Ni_{1-x}Zn_xFe_2O_4$", J. Magn. Magn. Mater., vol. 312, p. 210, 2007.

[3] A. Goldman, Handbook of Modern Ferromagnetic Materials, Kulwer Academic Publishers, Boston, USA, 1999.

[4] R. Valenzuela, Magnetic Ceramics, Cambridge University Press, Cambridge, 1994.

[5] W. Schiessl, W. Potzel, H. Karzel, M. Steiner, G. M. Kalvius, "Magnetic properties of the $ZnFe_2O_4$ spinel", Phys. Rev. B, vol. 53, p. 9143, 1996.

[6] Y. G. Chukalkin, A. E. Teplykh, "Magnetic state of nickel-zinc ferrites at high zinc concentrations", Phys. Solid State, vol. 40 (8), p. 1364, 1998.

[7] M. A. Ahmed, N. Okasa, L. Salah, "Influence of yttrium ions on the magnetic properties of Ni–Zn ferrites", J. Magn. Magn. Mater., vol. 264, p. 241, 2003.

[8] N. Rezlescu, E. Rezlescu, C. Pasnicu, M. L. Craus, "Effects of the rare-earth ions on some properties of a nickel-zinc ferrite", J. Phys. Condens. Matter, vol. 6, p. 5707, 1994.

[9] O. F. Caltun, L. Spinu, A. Stancu, "Structure and magnetic properties of Ni-Zn-Cu ferrites sintered at different temperatures", J. Optoelectron. Adv. Mater., vol. 4 (2), p. 337, 2002.

[10] S. T. Mahmud, A. K. M. Akther Hossain, A. K. M. Abdul Hakim, M. Seki, T. Kawai, H. Tabata, "Influence of microstructure on the complex permeability of spinel type Ni–Zn ferrite", J. Magn. Magn. Mater., vol. 305, p. 269, 2006.

[11] E. Rezlescu, L. Sachelarie, P. D. Popa, N. Rezlescu, "Effect of Substitution of Divalent Ions on the Electrical and Magnetic Properties of Ni–Zn–Me Ferrites", IEEE Trans. Magn., vol. 36, p. 3962, 2000.

[12] K. S. Amarendra, T. C. Goel, R. G. Mendiratta, "Magnetic properties of Mn-substituted Ni–Zn ferrites", J. Appl. Phys., vol. 92, p. 3872, 2002.

[13] R. Kulkarni Suresh, "Development of In^{3+} substituted Mn-Ni-Zn nanoferrite core material", Arch. Phys. Res., vol. 3(2), p. 116, 2012.

[14] M. M. Eltabey, W. R. Agami, H. T. Mohsen, "Improvement of the magnetic properties for Mn–Ni–Zn ferrites by rare earth Nd^{3+} ion substitution", J. Adv. Res., vol. 5, p. 601, 2014.

[15] W. O. Choi, W. H. Kwon, J. G. Lee, B. S. Kang, K. P. Chae, "Structural and Magnetic Properties of Nanoparticle Mn-Zn-Ni Ferrite Powders Grown by Using a Sol-gel Method", J. Korean Phys. Soc., vol. 61(11), p. 1812, 2012.

[16] K. S. Amarendra, A. Verma, O. P. Thakur, C. Prakash, T. C. Goel, R. G. Mendiratta, "Electrical and magnetic properties of Mn–Ni–Zn ferrites processed by citrate precursor method", Mater. Lett., vol. 57(5), p. 1040, 2003.

[17] E. Shirsath Sagar, B. G. Toksha, R. H. Kadam, S. M. Patange, D. R. Mane, S. Jangam, Ganesh, Ghasemi Ali, "Doping effect of Mn^{2+} on the magnetic behavior in Ni–Zn ferrite nanoparticles prepared by sol–gel auto-combustion", J. Phys. Chem. Sol., vol. 71(12), p. 1669, 2010.

[18] A. A. Sattar, H. M. El-Sayed, K. M. El-Shokrofy, M. M. El-Tabey, "Effect of Manganese Substitution on the Magnetic Properties of Nickel-Zinc Ferrite", J. Mater. Eng. and Perform., vol. 14(1), p. 99, 2005.

[19] A. A. Sattar, H. M. El-Sayed, K. M. El-Shokrofy, M. M. El-Tabey, "Improvement of the Magnetic Properties of Mn-Ni-Zn Ferrite by the Non-magnetic Al^{3+}-Ion Substitution", J. Appl. Sci., vol. 5(1), p. 162, 2005.

[20] M. I. Mendelson, "Average Grain Size in Polycrystalline Ceramics", J. Am. Ceram. Soc., vol. 52 (8), p. 443, 1969.

[21] A. K. M. Akther Hossain, H. Tabata, T. Kawai, "Magnetoresistive properties of $Zn_{1-x}Co_xFe_2O_4$ ferrites", J. Magn. Magn. Mater., vol. 320, p. 1157, 2008.

[22] R. Arulmurugan, B. Jeyadevan, G. Vaidyanathan, S. Sendhilnathan, "Effect of zinc substitution on Co–Zn and Mn–Zn ferrite nanoparticles prepared by co-precipitation", J. Magn. Magn. Mater. vol. 288, p. 470, 2005.

[23] P. P. Hankare, V. T. Vader, N. M. Patil, S. D. Jadhav, U. B. Sankpal, M. R. Kadam, B. K. Chougule, N. S. Gajbhiye, "Synthesis, characterization and studies on magnetic and electrical properties of Mg ferrite with Cr substitution", Mater. Chem. Phys., vol. 113, p. 233, 2009.

[24] J. Huang, "Microstructure and Properties of $Ni_{0.5}Zn_{0.5}Fe_2O_4$-$BaTiO_3$ Ceramic", Key Engineering Materials, vol. 336-338, p. 779, 2007.

[25] G. T. Rado, R. W. Wright, W. H. Emerson, A. Terris, "Ferromagnetism at Very High Frequencies. IV. Temperature Dependence of the Magnetic Spectrum of a Ferrite", Physical Review, vol. 88, p. 909, 1952.

[26] B. S. Chauhan, R. Kumar, K. M. Jadhav, M. Singh, "Magnetic study of substituted Mg–Mn ferrites synthesized by citrate precursor method", J. Magn. Magn. Mater., vol. 283, p. 71, 2004.

[27] J. L. Snoek, "Dispersion and absorption in magnetic ferrites at frequencies above one Mc/s", Physica, vol. 14, p. 207, 1948.

[28] S. A. Jadhav, "Magnetic properties of Zn-substituted Li-Cu ferrites", J. Magn. Magn. Mater., vol. 224, p. 167, 2001.

[29] L. Neel, Physica, "Nouvelle théorie du champ coercitif", vol. 15, p. 225, 1949.

[30] J. Smit, H. P. J. Wijn, Ferrites, John Wiley & Sons, New York, 1959.

[31] B. R. Karche, B. V. Khasbardar, A. S. Vaingankar, "X-ray, SEM and magnetic properties of Mg-Cd ferrites", J. Magn. Magn. Mater., vol. 168, p. 292, 1997.

[32] P. G. Bercoff, H. R. Bertorello, "Localized canting effect in Zn-substituted Ni ferrites", J. Magn. Magn. Mater., vol. 213, p. 56, 2000.

[33] J. Smit, Magnetic properties of materials, Mc-Graw Hill, New York, 1971.